TRITRON PROGRESS REPORT

W. Assmann, U. Buhl, A. Cazan, T. Grundey, G. Hinderer,
J. Junger, H.-J. Körner, R. Kratz, M. Leu, C. Rieß, L. Rohrer,
P. Schütz, U. Trinks, Ch. Yan

Technical University of Munich and University of Munich,
D-8046 Garching, W-Germany

ABSTRACT

The Tritron is a superconducting separated orbit cyclotron with strong transversal and rather strong longitudinal focusing. The project was finally funded in Juli 1987. The building, the cryostat and the refrigerator exist. The magnets for the beam transfer-lines and the accelerating cavities are ordered. Field measurements on test magnet channels gave satisfactory results, which may be further improved. The present quality factor of the superconducting prototype cavity exceeds the design value by a factor of 2. The voltage limit at 140 kV is probably due to multipacting not observed before at this level.

INTRODUCTION

At the Munich Accelerator Laboratory the Tritron is under construction. It will be a booster for the existing MP tandem[1]. It shall increase the ion energies by a factor of 4.9. Fig. 1 shows cross sections of the Tritron, Table 1 the main parameters.

The beam is led along a spiral orbit of almost 20 turns with constant turn separation Δr = 4 cm. Each of the 12 magnet sectors consists of 20 resp. 19 superconducting channels of the window frame type. In order to guide the bunches on the central path through the magnets, each channel can be adjusted individually by means of superconducting switches across the magnet coils[2]. The radial beam positions will be measured by beam profile monitors installed in each second intermediate sector. There are alternating gradients from one sector to the other to get strong focusing in both transversal directions. Six superconducting resonators operating at 170 MHz shall accelerate the ion bunches along the 20 parallel turns. To get longitudinal focusing, the bunches have to cross the cavities at a rf-phase with increasing voltage. The beam is injected through three superconducting channel magnets, the last with a bending radius of 300 mm corresponding to a field up to ~2 T. This magnet will limit the maximum attainable energy.

The whole machine is hanging under a torus like helium reservoir on the upper half of the cryostat. The cavities and magnets are cooled indirectly by pipes connected to the torus (thermal siphon cooling). There is no special vacuum system for the beam or the cavities. The cryostat including the torus exists. The stand-by losses of the cryostat are less than 5 W. A refrigerator (150 W at 4.7 K) and all transfer lines are installed.

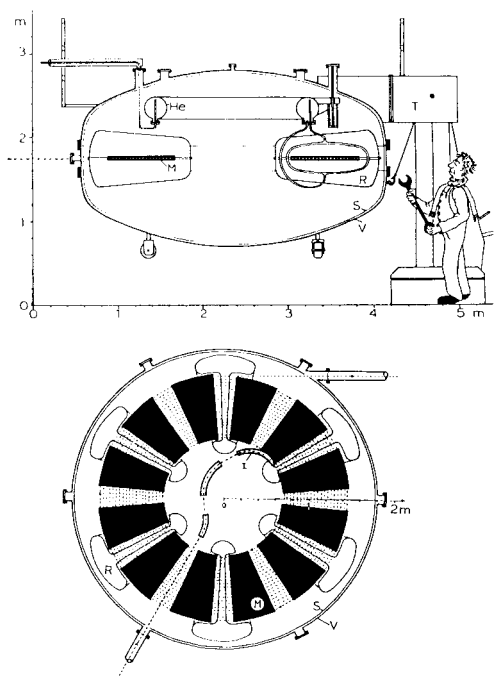

Fig. 1 Tritron cross sections. M: magnets; R: resonators; V: vacuum vessel; S: 80 K shield; He: liquid helium reservoir; T: support.

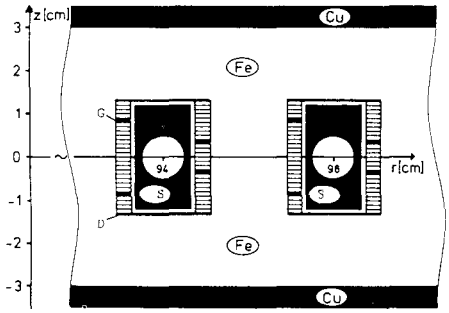

Fig. 2 Vertical cross section of a magnet sector. G: gradient windings; S: Cu shield; D: dead insulating layers.

MAGNETS

The magnet sectors consist of two steel sheets with slots every 4 cm (fig. 2). The sectors are mechanically identical up to the coils generating the alternating gradient. The coils are wound by a computer controlled winding machine (one channel /day) directly into the slots and then potted. They are shielded from beam losses by Cu profiles leaving a beam hole of diameter 11 mm. The coils are supported by the copper profiles and disc springs between.

The dimensions of the Tritron magnets are about one order of magnitude less than the accelerator magnets constructed before. Correspondingly the requirements or the tolerances are rather tight. Up to now seven channels for test purposes were produced. A maximum current of 1840 A was achieved without training, which is well above the design value (fig. 3).

The effective magnetic length measured by Hall probes is in good agreement with TOSCA calculations. The stray field 35 mm in front of the end plates is less than 0.5 G, so no problems due to frozen-in-flux in the superconducting layers of the cavities are expected.

To analyse higher order components in the radial field expansion narrow, bent superconducting induction loops were used, measuring the change of the magnetic length if the radial position x is varied. Three channels were investigated in detail with corresponding results, demonstrating the reproducibility of the

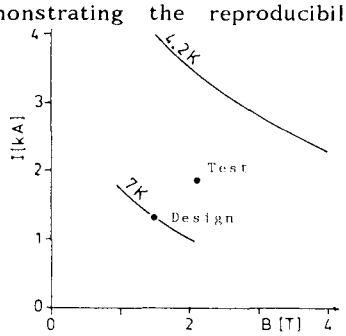

Fig. 3 Critical current limits at 4.2 and 7 K versus field, design current and test results.

Table 1: Tritron design data

Injector		13 MV tandem
Max. energy	H^{1+} (Q/A=1)	43.5 MeV
	S^{16+} (Q/A=0.5)	20.1 MeV/u
	Ag^{32} (Q/A=0.29)	7.6 MeV/u
Injection/extractions radius		66 cm/145 cm
Turn separation Δr		4 cm
Harmonic numbers		18-53
Magnet sector data:		
Number of magnet channels		20 (19)
Sector angle		20°
Bending radius ρ_1, ρ_{20}		430 mm/942 mm
Maximum magnetic field B_{max}		1.4 T
Radial gradients $\frac{1}{B}\frac{\delta B}{\delta r}$		3.6 m^{-1}, -5.2 m^{-1}
Dimensions of the supercond. cable		0.7 x 2.9 mm^2
Number of strands		14
Strand diameter		0.4 mm
Strand material	Cu/NbTi	1.35
Maximum cable current I_{max}		1420 A
Cavity data:		
Gap width at injection/extraction		60 mm/130 mm
Rf-frequency		170 MHz
Maximum accelerating field E_{max}		4.7 MV/m
Maximum voltage at r_2		0.50 MV
Stored Energy		~1.7 J
Dissipated power P		6 W
Quality factor (unloaded) Q_o		$3 \cdot 10^8$
Beam power		≤ 200 W
Geometry factor G		60 Ω
Surface resistance $R_s = G/Q_o$		$2 \cdot 10^{-7}$ Ω

production process. A typical measurement of the effective length related to the central length at x=0 is shown in fig. 4. The sextupole component, at x=±4 mm, given by the deviation of the curve from the tangent at x=0, is less than $-4 \cdot 10^{-3}$, which is within the tolerable limit of $5 \cdot 10^{-3}$. Contributions come from the entrance and exit edges, from a slit between the two halfs of the coil due to different thermal contraction of the coil and the steel, and from the gradient windings. It may be further reduced by adding dead spaces at the upper resp. lower edges of the coil, which will produce positive sextupole contribu-

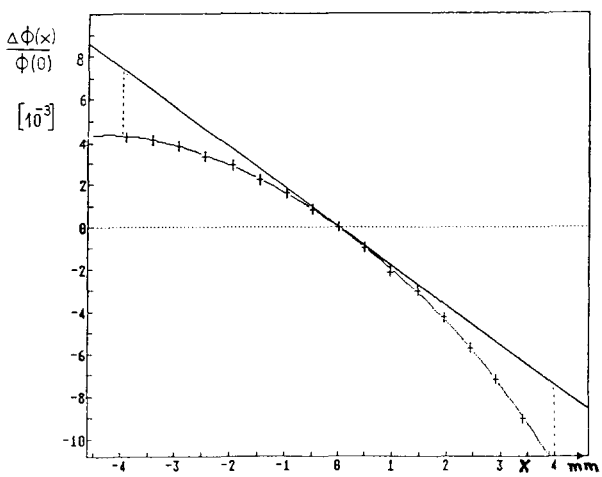

Fig. 4 Effective magnet length related to that at the magnet centre versus x. No current in the gradient coil.

tions (see fig. 2). A new test unit of three channels with such dead spaces has just been wound.
Presently the steel plates of all sectors are premilled, 1/3 of them are finally milled and ready for being polished. The superconducting cable exists, yet without insulation. The big winding machine is ready for first tests. A separate cryostat for testing single sectors is under construction.

THE SUPERCONDUCTING CAVITIES

The 6 wedge-shaped reentrant type resonators consist of half shells which are connected in the horizontal plane, so no currents will cross the joint. They are fabricated by electroplating copper (~10 mm) onto a fibre glass mould, which is destroyed and removed afterwards. The inner surface is electroplated with ~10 µm thick PbSn (2-4% Sn). The first cavity exists, the next will be delivered soon. Fig. 5 shows the radial voltage and accelerating field characteristics. The rf-superconductivity properties of PbSn were investigated systematically by means of a reentrant type cavity of rotational symmetry with 45 cm diameter and a frequency of 490 MHz in the fundamental mode[3]. The critical temperature of PbSn with ~2% Sn is 7.4 K compared to 7.2 K of Pb. The surface resistance R_S is the sum of R_{BCS} from the BCS-theory and the residual resistance R_{RES} due to imperfect surfaces (independent of temperature). R_S was measured at 4.2 K in the range from 490 to 1670 MHz by operating the cavity in different modes (fig. 6). The R_{BCS}-values were obtained from the temperature dependence of R_S. The fitted line gives a frequency dependence $\sim f^{1.9}$ compared to $f^{1.74}$ for Pb. The PbSn-line is about a factor of two below the Pb-line. The observed improvement can be explained by the influence of the electron mean free path on R_{BCS}. It is remarkable, that the residual resistances of the test cavity are not too far above the R_{BCS}-line, which may be due to the increased chemical stability of the alloy with respect to oxidation.
The surface resistance at 170 MHz in fig. 6 was obtained for the Tritron cavity with the best surface up

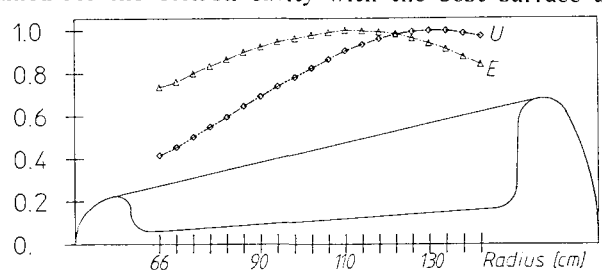

Fig. 5 Voltage and electrical field characteristic of the cavity in relative units and half of the horizontal cross section.

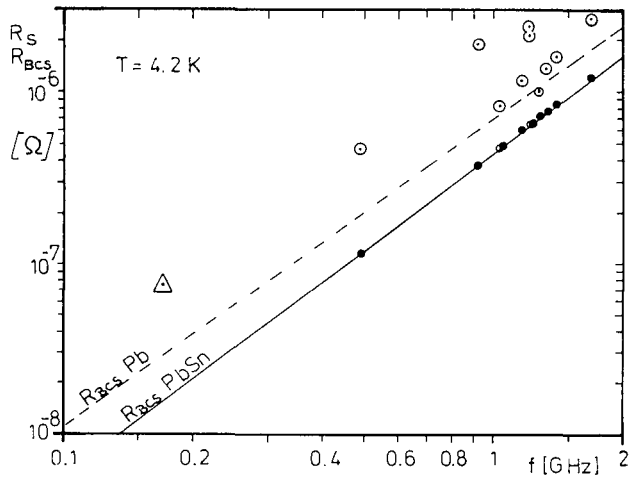

Fig. 6 Surface resistance R_S of the test cavity (⊙) at different modes above 490 MHz and of the Tritron cavity (△) at 170 MHz. The data on R_{BCS} (●) were obtained from the temperature dependence of R_S. Alloy: PbSn with ~2% Sn.

to now, prepared with several rinsing courses and fast drying by N_2-blast following the electroplating process. It fits rather well into the data taken at higher frequencies. The unloaded quality factor for this cavity is almost independent of the maximum voltage across the accelerating gap as shown in fig. 7, uppermost curve. The maximum voltage was limited by multipacting not observed at this level before. It probably is caused by a small piece of steel sticking on the cavity wall in a region of low electric field. Preceding tests with imperfect surface preparation gave Q_o-values decreasing with voltage (lower curve in fig. 7), may be due to oxidation. The maximum field obtained up to now was 5.4 MV/m. It was measured by observing

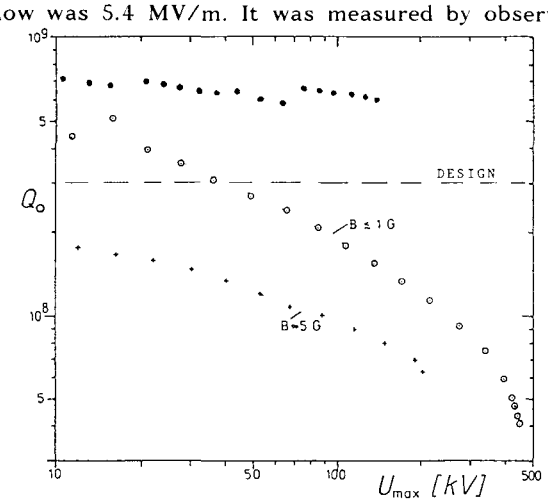

Fig. 7 Unloaded quality factor of the Tritron cavity versus the maximum gap voltage. Uppermost curve with improved PbSn (2% Sn) surface, external field < 1 G. Lower curves with imperfect surface

the energy gain of electrons from a ^{207}Bi source. Oscillations of the frequency caused by acoustic noise were less than 50 Hz. No ponderomotoric oscillations were observed.

BEAM DYNAMICS

The magnet sectors and cavities are arranged such, that the length of the central path from one cavity to the next increases constantly by the same amount. The central particle is led along the spiral orbit without any transversal deviations by adjusting all magnetic fields corresponding to the respective momentum. The longitudinal motion of the central particle is given by

$$\Delta T'' - b(m) \cdot \Delta T' + q(m) \cdot \Delta T = p(m) \qquad (1)$$

with m the turn number as independent variable; $\Delta T = T - T_{is}$ the energy deviation from the isochroneous energy T_{is}, which is defined for fixed rf-frequency by the condition of constant path length increase;
$b(m) = V_o'(m)/V_o(m)$ is the normalized change of the accelerating voltage amplitude;
$q(m) = [2\pi h/\gamma(\gamma+1)T_{is}] \cdot \sqrt{(Q/A \cdot V_o)^2 - T_{is}'^2 \cdot -[2T_{is}' \Delta T + \Delta T'^2]}$
is a predetermined function, if the last term within brackets can be neglected; h being the harmonic number;
$p(m) = T_{is}' V_o'/V_o - T_{is}''$ is a given function too.
If $\Delta T'$ is sufficiently small, the solution of equation (1) is a superposition of a smooth equilibrium function « T_{is} (particular integral of (1), which can be written as infinite power series, approximatively given by $p(m)/q(m)$) and an oscillation with varying amplitude and frequency (solution of the corresponding homogeneous equation), which represents coherent synchrotron oscillations without transversal excursions of the bunch. Depending on the initial energy and rf-phase the oscillations may vanish leaving the equilibrium

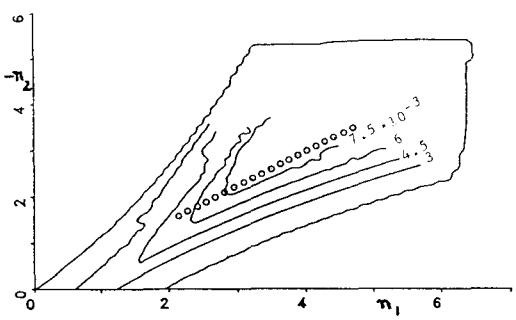

Fig. 8 Stability diagram and working line. n_1, n_2 field indices of axially resp. radially focusing channels. Included are stability limits for different sextupole contributions at x = ±4 mm, calculated for transversal emittances of 6 π mm mrad.

solution. The oscillation numbers $Q_{coh} \sim 0.3$ per turn, mainly determined by $\sqrt{q(m)}$, are somewhat larger than $Q_{incoh} \sim 0.2$, the incoherent synchrotron oscillation numbers of off-centre ions circulating the bunch centre[4]. To get longitudinal focusing for the off-centre ions, the phase φ of the central particle has to stay below π/2. Depending on the central phase the amplitude of the coherent energy oscillations can amount to some % of T_{is}, so that a limited energy variation is possible, even though the rf-frequency and harmonic number is fixed. Therefore the cavities will be equiped with a fine tuning system only.
The above results were verified by means of a computer code. As a further result of these calculations may be mentioned, that the Tritron can be operated even if one cavity is switched off.
To fix the working line with respect to the field indices n_1 and n_2, the limits of the stability diagram were calculated (fig. 8). The working line is directed from right below to the left, if all radially focusing channels with n_2 are operated with out current and all axially focusing channels with n_1 at the same current of ~500 A (increasing n_1). Then the betatron oscillation numbers vary from $Q_x(1) \approx 1.2$ to $Q_x(20) \approx 1.6$ and $Q_z(1) \approx 0.9$ to $Q_z(20) \approx 1.9$. Resonances are crossed too fast to become effectively. Included in the diagram are limiting lines of constant tolerable sextupole contributions (assumed to be constant in all channels). From this the upper limit of $\sim 5 \cdot 10^{-3}$ for the relative sextupole component at x = ± 4 mm can be deduced. The transversal defocusing of the cavities, caused mainly by the radially directed electrical field components at the entrance and exit of the almost circular beam holes, shifts the working line only slightly.

This work has been funded by the German Federal Minister of Research and Technology (BMFT) under the contract number 06 TM 855.

REFERENCES

1) Trinks, U., Assmann, W. and Hinderer, G., Nucl. Instr. and Meth. in Phys. Research, A244 (1986) 273-282
2) Savoy, R., Thesis, Techn. Univ. Munich, July 1988
3) Dietl, L., Thesis, Techn. Univ. Munich, 1988, to be published in N.I.M.
4) Hinderer, G., Proceedings of the 11th Intern. Conf. on Cyclotrons and their Applications, 1986, pp. 215-221